

Large suppression of quantum fluctuations of light from a single emitter by an optical nanostructure

Diego Martín-Cano,^{1,3} Harald R. Haakh,¹ Karim Murr^{2,3,4,5} and Mario Agio^{2,3,4}

¹*Max Planck Institute for the Science of Light, 91058 Erlangen, Germany*

²*National Institute of Optics (CNR-INO), 50125 Florence, Italy*

³*Center for Quantum Science and Technology in Arcetri (QSTAR), 50125 Florence, Italy*

⁴*European Laboratory for Nonlinear Spectroscopy (LENS), 50019 Sesto Fiorentino, Italy*

⁵*Dipartimento di Fisica ed Astronomia, Università di Firenze, 50019 Sesto Fiorentino, Italy*

We investigate the reduction of the electromagnetic field fluctuations in resonance fluorescence from a single emitter coupled to an optical nanostructure. We find that such hybrid system can lead to the creation of squeezed states of light, with quantum fluctuations significantly below the shot noise level. Moreover, the physical conditions for achieving squeezing are strongly relaxed with respect to an emitter in free space. A high degree of control over squeezed light is feasible both in the far and near fields, opening the pathway to its manipulation and applications on the nanoscale with state-of-the-art setups.

PACS numbers: 42.50.Lc, 42.50.Dv, 78.67.-n, 42.50.Ar

I. INTRODUCTION

Optical nanostructures are known to be efficient architectures for controlling light-matter interactions.¹ In this context, the most widely considered processes have been Raman scattering and fluorescence, whose enhancement has been experimentally verified at the single-emitter level.^{2–4} A major goal is now to explore their performance in the quantum regime,⁵ so far mainly examined in cavity quantum electrodynamics.⁶ Antibunching has been investigated as a signature of the granularity of quantum light arising from single emitters coupled to nanostructures.^{7–9} In contrast, electromagnetic field fluctuations below shot noise,¹⁰ which mirror the quantum wave nature of light, are known to be challenging to measure¹¹ at the quantum level and have not been addressed in such hybrid systems.

Reduced quantum fluctuations are the unique characteristics of squeezed states of light,¹² which are relevant for overcoming classical application limits in, for instance, precision measurements, spectroscopy and optical communications. Despite recent advances on the microscopic scale,^{11,13} sources of squeezed light usually rely on the nonlinear response of macroscopic systems, typically crystals or atomic vapors.¹⁴ Although optical nanostructures exhibit classical field statistics in the linear regime, they are able to fundamentally alter the radiation properties of a quantum emitter (QE) placed at close proximity.¹ This approach can be applied in a broad range of nanoarchitectures and QEs, covering atoms,¹⁵ color centers,^{8,9} molecules,^{3,4} or quantum dots.⁷ An interesting question is thus to what extent the coupling between a nanostructure and a QE can modify the electromagnetic field fluctuations.

Here, we show that nanostructures can significantly increase squeezing in the resonance fluorescence from a QE. Moreover, they strongly relax the conditions for overcoming shot noise in terms of bandwidth and excitation power. Our results open a pathway towards the experimental measurement of such squeezed states of light in state-of-the-art setups and their manipulation on the nanoscale, with prospects for advancing applications at the single-photon level.

II. DISCUSSION

Method. Electromagnetic field fluctuations can be measured by homodyne techniques,¹⁶ which detect the variance of the electric field quadrature component $\hat{E}_i(\mathbf{r}, t) = \hat{E}_i^{(+)}(\mathbf{r}, t) + \hat{E}_i^{(-)}(\mathbf{r}, t)$, given by $(\Delta\hat{\mathcal{E}}_i)^2 = \langle :(\hat{E}_i - \langle \hat{E}_i \rangle)^2: \rangle$. Here, we consider the normal ordering ($::$) to directly compare the variance to the shot-noise level, so that negative values of $(\Delta\hat{\mathcal{E}}_i)^2$ indicate squeezed light. We evaluate these fluctuations in the framework of macroscopic quantum electrodynamics in dispersive and absorptive media.¹⁶ In the case of a two-level QE and imposing the rotating wave and Markov approximations, the positive-frequency scattered electric field operator is $\hat{E}_i^{(+)}(\mathbf{r}, t) = |g_i(\mathbf{r})|e^{i\phi_i(\mathbf{r})}\hat{\sigma}(t)$, which depends on the QE coherence $\hat{\sigma} = |g\rangle\langle e|$. Here, $|g\rangle$ and $|e\rangle$ are the QE's ground and excited states, respectively. The emission characteristics in the presence of a given nanoarchitecture are encoded in the amplitude $|g_i|$ and phase ϕ_i , which can be expressed in terms of the classical electromagnetic Green's tensor¹⁷ (see details in Appendix A). Evaluating the fluctuations of $\hat{E}_i(\mathbf{r}, t)$ we find

$$(\Delta\hat{\mathcal{E}}_i(\mathbf{r}, t))^2 = 2|g_i(\mathbf{r})|^2 \left[\langle \hat{\sigma}^\dagger(t)\hat{\sigma}(t) \rangle - |\langle \hat{\sigma}(t) \rangle|^2 - \text{Re} \left(e^{i2\phi_i(\mathbf{r})} \langle \hat{\sigma}(t) \rangle^2 \right) \right]. \quad (1)$$

The expectation values are then replaced by the solution of the optical Bloch equations under steady-state conditions. These contain the effects of the driving field's Rabi frequency Ω , the spontaneous decay at a rate γ , and the frequency detuning $\delta_L = \omega_L - \tilde{\omega}_E$ between the laser and

the QE. The nanostructure affects all of these via a local field enhancement and a shift in the QE resonance to a value $\tilde{\omega}_E$. We also allow for additional pure dephasing at a rate γ^* .¹⁶ In this case, Eq. (1) can be expressed in a form valid for a QE in any environment

$$(\Delta\hat{\mathcal{E}}_i(\mathbf{r}, t))^2_{\text{steady state}} = |g_i(\mathbf{r})|^2 \frac{z^2}{1 + \delta^2 + z^2} \left(1 - \frac{(\delta^2 + 1)(1 + \cos[2\phi_i + 2\Phi - 2\omega_L t])}{(1 + x)(1 + \delta^2 + z^2)} \right), \quad (2)$$

expressed in terms of the normalized dephasing rate $x = 2\gamma^*/\gamma$, the normalized detuning $\delta = 2\delta_L/(\gamma + 2\gamma^*)$, and the normalized Rabi frequency $z = \sqrt{2}|\Omega|/\sqrt{\gamma(\gamma + 2\gamma^*)}$, associated with the QE's saturation parameter. The cosine in Eq. (2) can be set to unity without loss of generality.¹⁸ A detailed derivation of Eqs. (1) and (2) are given in Appendix B.

A hybrid nanosystem. From Eq. (1), we see that the electric field fluctuations generated by a QE in resonance fluorescence are governed by the emitter's optical coherence $\hat{\sigma}$ and upper-state population $\hat{\sigma}^\dagger\hat{\sigma}$.¹⁰ The fluctuations $\langle \hat{\sigma}^\dagger(t)\hat{\sigma}(t) \rangle - |\langle \hat{\sigma}(t) \rangle|^2$ are always positive, and, hence, tend to destroy squeezing, but they approach zero the weaker the excitation. Since we deal with one QE, this results in low photon count rates, which has prevented the detection of fluctuations below shot noise in free space and made it challenging even in the presence of a resonator.¹¹ The last term in Eq. (1) originates from quantum fluctuations in the optical coherence. It is the only one able to create squeezing and cannot be interpreted neither with classical waves nor with particles alone, bearing out the quantum wave nature of this process. If a QE is placed near a nanostructure, the dynamics that generate quantum squeezing are fundamentally changed. First, both the amplitude $|g_i(\mathbf{r})|^2$ and the phase $\phi_i(\mathbf{r})$ of the field fluctuations are modified by the nanostructure due to its electromagnetic response. Hence, although the nanostructure increases the field intensity scattered by the QE,¹ its quantum fluctuations can be comparatively reduced with respect to shot noise, with a squeezing amplitude $|g_i(\mathbf{r})|^2$. Second, since the coherence $\hat{\sigma}$ is affected by the enhancement of the driving field and the change in the spontaneous decay rate, both induced by the nanostructure,¹ control of these magnitudes can be used to significantly reduce the electromagnetic field fluctuations in the emission from a QE, while increasing the photon count rate.

Far-field squeezing amplitudes. For a quantitative analysis, we exemplify the nanostructure with a gold nanosphere (GNS), coupled to a QE characterized by its

transition frequency $\omega_E = 2\pi c/\lambda_E$ and dipole \mathbf{d} , as illustrated in Fig. 1a. In this case, the Green's tensor \mathbf{G} is known analytically. In the far field ($|\mathbf{r} - \mathbf{r}_E| \gg \lambda_E$), $g_i = |g_i|e^{i\phi} \approx \frac{\omega_E^2}{\varepsilon_0 c^2} G_{ij}(\mathbf{r}, \mathbf{r}_E, \omega_E) d_j$ provides an excellent approximation of the amplitude and phase in Eq. (1), whereas a quantum correction must be included in the near field¹⁹ (see further details in Appendix A). Figure 1b shows the squeezing amplitude $|g_\theta|^2$ at the detection point in the far field (D_1 in Fig. 1a), where the θ -component dominates. This amplitude features several local maxima, arising from the excitation of plasmon-polariton resonances,²⁰ which depend on the nanosphere radius R and on the QE emission wavelength λ_E . The strongest one originates from the dipole resonance, as indicated by the two-lobe pattern in the far field, shown in Fig. 1c. Notice that near the global maximum, squeezing is enhanced by a factor of 20 due to the presence of the nanosphere. Further maxima at larger radii are associated with higher-order resonances. Although they provide weaker enhancement, they reshape the far-field pattern more strongly than the dipolar one (see Fig. 1c). Therefore, nanostructures may be exploited to control the directionality of squeezed-state emission in the far field, which can be optimized by suitably designed architectures.²¹

Bounds of squeezing. The presence of the nanostructure also strongly modifies the conditions for the creation of squeezed light from a QE. This is possible because the field fluctuations depend on the frequency detuning δ_L between the QE and the driving field, the Rabi frequency Ω (*i.e.* the driving field) and the QE's spontaneous decay rate γ , which differ from their values in free space¹ (δ_{L0} , Ω_0 , and γ_0 , respectively). In practice, we observe that the boundaries for the generation of squeezing depend only on the ratios Ω/γ and δ_L/γ [see Eq. (2)]. For a QE-GNS configuration, these limits are shown in Fig. 2a as a function of the rescaled detuning and driving field ($\delta_0 = 2\delta_{L0}/\gamma_0$ and $z_0 = \sqrt{2}\Omega_0/\gamma_0$, respectively). Importantly, we find that the detuning range with sizable squeezing has increased by two orders of magnitude with

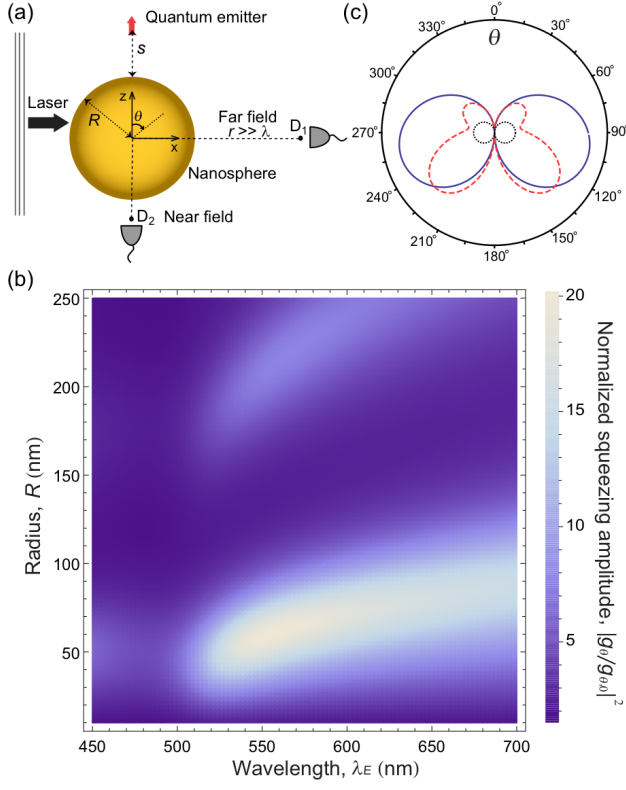


FIG. 1. (Color online) (a) Hybrid system consisting of a quantum emitter at a distance s from a gold nanosphere of radius R . D_1 and D_2 are the detection points in the far and near fields, respectively. D_1 is on the x -axis at a distance $10^5 \lambda_E$ from the nanosphere center, while D_2 is along the z -axis, 10 nm from the nanosphere surface. The emitter dipole moment is oriented perpendicularly to the nanosphere surface. (b) Normalized squeezing amplitude $|g_\theta/g_{\theta,0}|^2$ as a function of λ_E and R . For comparison, the squeezing amplitude is normalized with respect to its value in the absence of the nanosphere, $|g_{\theta,0}|^2$. The distance between the quantum emitter and the nanosphere surface is $s = 10$ nm. The detection point corresponds to D_1 as shown in panel (a). The θ -component of the field quadrature corresponds to the dominant polarization in this configuration. (c) Far-field squeezing amplitude $|g_\theta|$, near the dipolar ($R = 60$ nm, solid blue curve) and quadrupolar ($R = 120$ nm, dashed red curve) nanosphere resonances at $\lambda_E = 550$ nm. The dotted black curve corresponds to the free-space case.

respect to the case in free space, as displayed in Fig. 2b. This is directly related to the enhancement of the QE spontaneous decay rate $\gamma/\gamma_0 \sim 60$ by the GNS, which also leads to a shift in the resonance frequency. Moreover, the nanostructure strongly influences the local field intensity at the position of the QE, so that squeezing occurs over a much wider range of laser intensities as compared to free space, *c.f.* Fig. 2b at zero detuning. The reason is that the GNS has a larger impact on the QE decay rate than on the driving field enhancement with respect to free space ($\Omega/\Omega_0 \sim 4.9$ for this case), so that

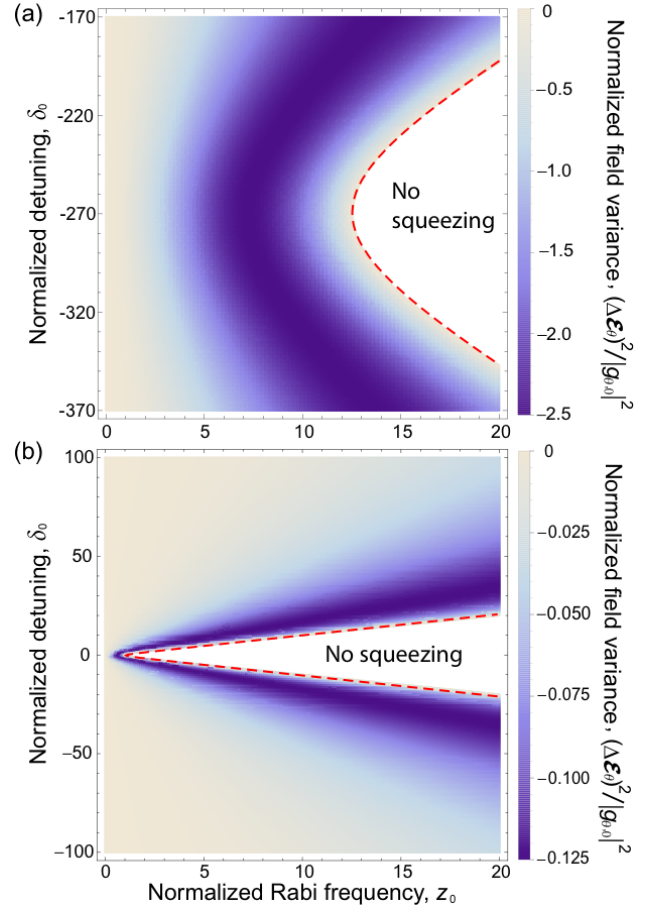


FIG. 2. (Color online) Electric field fluctuations in the presence (a) and in the absence of a nanosphere (b). The relevant system parameters are $s = 10$ nm, $R = 60$ nm, $\lambda_E = 550$ nm and fields are detected at D_1 (see Fig. 1a). For comparison, the variances are normalized by the squeezing amplitude in free space $|g_{\theta,0}|^2$. Both panels cover equal ranges of detuning and driving laser intensity. Moreover, the lower bound of the color scale displays the different minimum value in each panel. Their ratio emphasizes the 20-fold enhancement of squeezing due to the nanosphere as compared to free space.

the ratio Ω/γ provides a weaker excitation level at the same incident power ($\propto z_0 \Omega/\gamma$).

Reduced quantum fluctuations under dephasing. Realistic QEs in free space are strongly affected by dephasing,²² which can preclude the generation of squeezing. To gain intuition on how the nanostructure may overcome this difficulty, we show in Fig. 3 the field fluctuations $(\Delta \hat{\mathcal{E}}_\theta)^2$ as we vary the distance s between the QE and the GNS surface (see Fig. 1a) at zero detuning, fixed Rabi frequency, and assuming an additional constant rate of pure dephasing, $\gamma^* = \gamma_0/2$. In free space, $(\Delta \hat{\mathcal{E}}_\theta)^2$ exhibits small positive values, *i.e.* the field fluctuations lie above shot noise. In contrast, the presence of the GNS allows for quantum squeezing over a range of distances s that depend on the Rabi frequency, on the

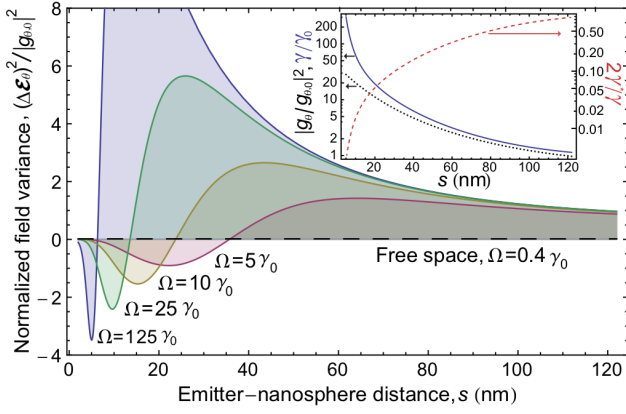


FIG. 3. (Color online) Normalized electric field fluctuations for the θ -component as a function of the distance s between the quantum emitter and the nanosphere surface. The quantum emitter is affected additionally by pure dephasing at a rate $\gamma^* = \gamma_0/2$. The curves corresponds to Rabi frequencies $\Omega = 5\gamma_0, 10\gamma_0, 25\gamma_0$, and $125\gamma_0$, respectively. The other system parameters are the same as in Fig. 2a. For comparison, the result in the absence of the nanostructure and $\Omega = 0.4\gamma_0$ is represented by the black dashed line. The inset shows the normalized total decay rate γ/γ_0 (solid blue curve, left axis) and the field intensity enhancement factor $|g_\theta/g_{\theta,0}|^2$ (dotted black curve, left axis) as a function of s . The ratio $2\gamma^*/\gamma$ between the additional pure dephasing and the one associated with spontaneous decay is also displayed (dashed red curve, right axis).

dephasing rate and on the spontaneous decay. For example, for $\Omega = 5\gamma_0$, negative values of $(\Delta\mathcal{E}_\theta)^2$ occur below $s = 35$ nm and its minimum is reached at $s = 23$ nm. This overall behavior is general, as highlighted by the other curves in Fig. 3 corresponding to larger Rabi frequencies. The minimum of each curve results from a balance between the Rabi frequency, the decay rate γ , the ratio $2\gamma^*/\gamma$, and the amplitude g_i . All of these depend on the emitter position (see the inset of Fig. 3) while the Rabi frequency is kept constant. Importantly, it is the large increase in the fluorescence rate γ with respect to the free-space rates γ^* and γ_0 that helps to fulfill the condition for squeezing in Eq. (2).²³ As the QE moves towards the GNS surface, optimal squeezing requires increasingly stronger driving fields, especially once the distance s falls below 10 nm, where absorption by real metals provides a dominating nonradiative decay channel for the QE.²⁴ This is reflected in the growing deviation of γ/γ_0 from the normalized radiative amplitude of squeezing $|g_\theta/g_{\theta,0}|^2$ (see inset in Fig. 3). Nevertheless, the ratio between radiative and nonradiative decay can be modified by optimized nanostructures²⁴ and quantum squeezing may, in principle, be enhanced without considerably raising the driving strengths to compensate for the nonradiative losses. Thus the coupling of a QE to a nanostructure may facilitate the creation of squeezed states of light despite of decoherence.

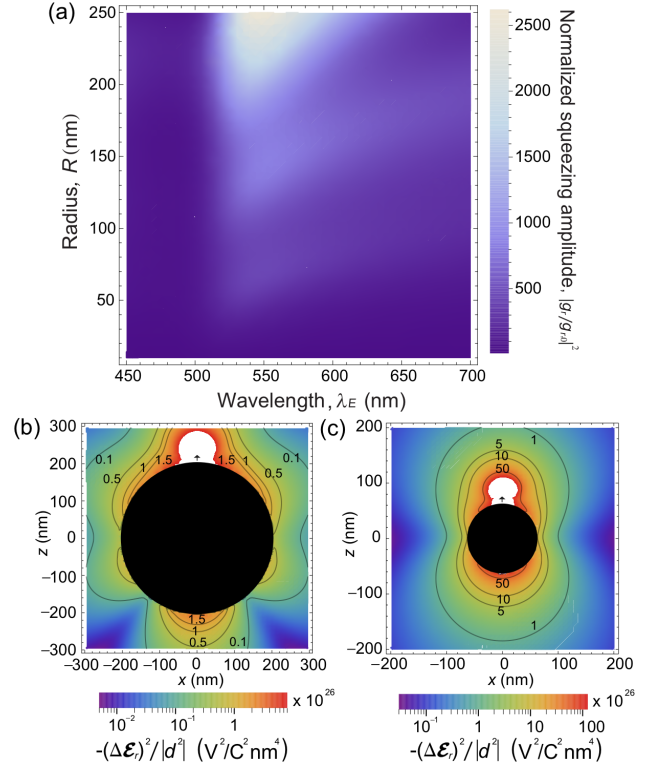


FIG. 4. (Color online) (a) Normalized squeezing amplitude for the radial near-field component $|g_r/g_{r,0}|^2$ as a function of λ_E and R , for an emitter-surface distance $s = 10$ nm and detection at D_2 (see Fig. 1a). (b-c) Contour maps of the negative field fluctuations for the radial component for $R = 200$ nm (b) and $R = 60$ nm (c), with $s = 10$ nm and $\lambda_E = 550$ nm. The values are normalized to the square modulus of the dipole moment $|\mathbf{d}|^2$ to be independent of a specific quantum emitter. The emitter and the nanosphere are represented by a black arrow and a disk in the xz -plane, respectively.

Reduced quantum fluctuations in the near field. Further enhancement of squeezing can be achieved in the near field, where intense evanescent modes become relevant. We emphasize that even in free space, the squeezing amplitude close to a QE is orders of magnitude higher as compared to the far field, due to the spatial behavior of its dipolar field.²⁵ To estimate the ability of nanostructures to transport squeezed light away from the QE, we consider a detection point on the opposite side of the GNS (D_2 in Fig. 1a). Figure 4a displays the normalized squeezing amplitude for the radial field component, $|g_r/g_{r,0}|^2$, which dominates in the near-field region. The enhancement leads to values two orders of magnitude larger than those encountered in the far field in the same parameter space explored by varying the wavelength λ_E and the radius R . In contrast with the far-field, the enhancement of squeezing increases with higher-order plasmon-polariton resonances at larger radii. This fact arises from the rapid spatial decay of the radial field in free space combined with the field enhancement near

the GNS surface, which boosts the ratio $|g_r/g_{r,0}|^2$. Intuitively, we expect this quantity to increase up to very high radii until the system resembles a QE near a flat metal surface, where it becomes limited by propagation losses over the system size.¹⁹

For a better understanding of the strong spatial dependence of the squeezing amplitude in the near field, we now analyze the electric field fluctuations over a cross-section of the surrounding of the GNS. Figure 4b gives the near-field squeezing pattern for a large GNS ($R = 200$ nm). We observe two lateral lobes, which stem from the excitation of higher-order plasmon-polariton resonances. Such squeezed field modes are superimposed with the dipolar contribution indicated by the presence of the top and bottom lobes, which are more clearly visible in Fig. 4c in the case of a smaller GNS ($R = 60$ nm), for which the dipole resonance prevails. Note that despite the huge enhancements found for large GNSs compared to free space (see Fig. 4a), the small GNS improves the squeezing amplitude, *e.g.*, by a factor 30. This is the result of a shorter detection distance with respect to the QE combined with a higher near-field enhancement.

III. CONCLUSIONS

Our study indicates a wide range of possibilities for controlling the quantum fluctuations of light at the nanoscale using a laser-driven QE coupled to a nanoarchitecture. We found that the nanostructure-assisted

dynamics of a QE improves the generation of squeezed light in resonance fluorescence, overcoming the limitations of weak driving. An antenna effect⁴ allows for boosting the transfer of squeezing to the far field, resulting in a large suppression of quantum fluctuations. The huge enhancement of spontaneous decay made possible by optical nanostructures²⁴ may also allow for the generation of squeezed states of light under conditions where the system undergoes fast dephasing. Altogether, these findings facilitate the detection of quantum squeezing in resonance fluorescence from a single emitter within the possibilities of current experiments and provide perspectives for its practical application. For instance, the large near fields can generate quantum fields on the nanoscale with squeezing levels that are orders of magnitude higher than in the far field. These could be efficiently transferred over a considerable distance by nanoscale waveguides.²⁶ Furthermore, since our approach can be applied to many different types of quantum emitters and nanostructures, it may help to develop novel solid-state sources of squeezed light for integrated nanophotonic systems⁷⁻⁹ and quantum-limited sensitivity,^{14,27} and provide new insights into the production of multi-partite entangled states.^{28,29}

ACKNOWLEDGMENTS

Financial support from the Max Planck Society, the EU-STREP project “QIBEC” and the MIUR-PRIN grant (2010LLKJBX) are gratefully acknowledged. M.A. wishes to thank Vahid Sandoghdar.

Appendix A: Electric field operator for the composite system

We use the macroscopic quantum electrodynamics formalism of Knöll *et al.* [30] to write the operator $\hat{\mathbf{E}}^{(+)}(\mathbf{r}, t)$ of the positive-frequency electric field scattered by a single quantum emitter, modeled as a two-level system (TLS), coupled to a nanostructure of arbitrary shape. These electric field operators can be used to obtain the correlations that identify the generation of squeezed light, which are derived in Appendix B. Within the rotating wave approximation, the electric field operator is written in terms of the electromagnetic Green’s tensor \mathbf{G} and the emitter lowering operator $\hat{\sigma}$ as

$$\begin{aligned}\hat{\mathbf{E}}_{\text{tot}}^{(+)}(\mathbf{r}, t) &= \hat{\mathbf{E}}_{\text{free}}^{(+)}(\mathbf{r}, t) + \hat{\mathbf{E}}^{(+)}(\mathbf{r}, t), \\ &= \hat{\mathbf{E}}_{\text{free}}^{(+)}(\mathbf{r}, t) + \frac{i}{\pi\epsilon_0} \int_0^\infty d\omega \frac{\omega^2}{c^2} \text{Im}\{\mathbf{G}(\mathbf{r}, \mathbf{r}_E, \omega)\} \cdot \mathbf{d} \int_{t'}^t d\tau e^{-i\omega(t-\tau)} \hat{\sigma}(\tau),\end{aligned}\quad (\text{A1})$$

where the first term represents the freely evolving part of the driving electric field and the second term corresponds to the source part scattered by the composite system. The quantum emitter is located at \mathbf{r}_E and is characterized by its emission frequency ω_E and its transition dipole matrix element \mathbf{d} . The Markov approximation, in which $t' \rightarrow -\infty$, holds for intervals $t - t'$ larger than the short correlation times in the presence of the nanostructure, so that the electric field operator can be expressed as³⁰

$$\hat{\mathbf{E}}_{\text{tot}}^{(+)}(\mathbf{r}, t) = \hat{\mathbf{E}}_{\text{free}}^{(+)}(\mathbf{r}, t) + i\hbar\hat{\sigma}(t) (\gamma(\mathbf{r})/2 + i\delta\omega(\mathbf{r})), \quad (\text{A2})$$

where

$$\delta\omega(\mathbf{r}) = \frac{\mathcal{P}}{\pi\hbar\epsilon_0} \int_0^\infty d\omega \frac{\omega^2}{c^2} \frac{\text{Im}\{\mathbf{G}(\mathbf{r}, \mathbf{r}_E, \omega)\} \cdot \mathbf{d}}{\omega_E - \omega}, \quad (\text{A3})$$

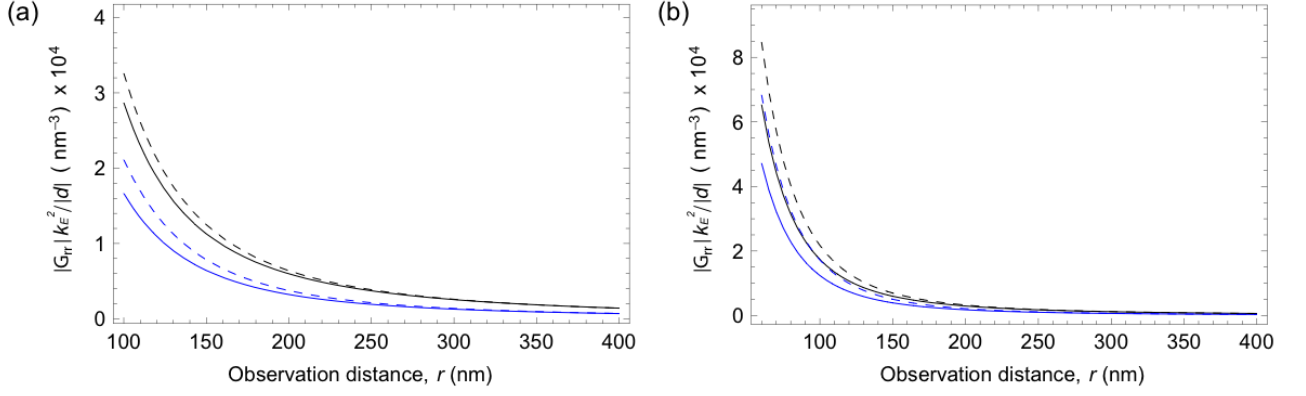


FIG. 5. Absolute value of the radial-radial component of the Green's tensor (dashed curves) and the full contribution to the radial component of the amplitude $|g_r|$ in Eq. (A2) (solid curves) as a function of the observation distance r for $R = 80$ nm (a) and $R = 45$ nm (b), and two different emission wavelengths, $\lambda = 600$ nm (black curves) and $\lambda = 800$ nm (blue curves), respectively. Their values are multiplied by the emission wavevector $k_E^2/|d|$ which corresponds to units of nm^{-3} . The emitter separation from the GNS corresponds to $s = 10$ nm, observation angle $\theta = \pi/2$ (see Fig. 1) and the emitter dipole-moment is perpendicular to the GNS surface.

and

$$\gamma(\mathbf{r}) = \frac{2\omega_E^2}{\hbar\epsilon_0 c^2} \text{Im}\{\mathbf{G}(\mathbf{r}, \mathbf{r}_E, \omega_E)\} \cdot \mathbf{d}, \quad (\text{A4})$$

are vectors and ω_E is the emitter resonance frequency.

We rewrite the source part of Eq. (A2) as a complex vector, the i th-component of which is proportional to the emitter lowering operator

$$\hat{E}_i^{(+)}(\mathbf{r}, t) = i\hbar\hat{\sigma}(t) (\gamma_i(\mathbf{r})/2 + i\delta\omega_i(\mathbf{r})) = |g_i(\mathbf{r})|e^{i\phi_i}\hat{\sigma}(t). \quad (\text{A5})$$

The amplitude corresponds to

$$|g_i(\mathbf{r})| = \hbar\sqrt{(\gamma_i(\mathbf{r})/2)^2 + (\delta\omega_i(\mathbf{r}))^2}, \quad (\text{A6})$$

and the complex phase is

$$\phi_i(\mathbf{r}) = \arctan\left(-\frac{\gamma_i(\mathbf{r})}{2\delta\omega_i(\mathbf{r})}\right). \quad (\text{A7})$$

In a general geometry, the amplitude involved in the source part of Eq. (A2) has to be evaluated numerically. A semi-analytical treatment of the Green's tensor is possible for the case of a gold nanosphere (GNS) considered in this work.^{31,32} In particular, the frequency integral in Eq. (A3) can be calculated in the complex plane, where the tabulated optical constants of gold³³ are replaced by a Drude-Lorentz dispersion model.³⁴

The principal value integral can be simplified by neglecting off-resonant contributions in the intermediate and far-field region ($|\mathbf{r} - \mathbf{r}_E| \gg \lambda$).^{35,36} The impact of this approximation can be seen in Fig. 5, where we compare the absolute values for the radial-radial Green's tensor components obtained from the exact integral ($I(\mathbf{r}, \mathbf{r}_E, \omega_E) = |\mathcal{P} \int d\omega [\text{Im}\{G_{rr}(\mathbf{r}, \mathbf{r}_E, \omega)\}/(\omega_E - \omega)] + i\text{Im}\{G_{rr}(\mathbf{r}, \mathbf{r}_E, \omega_E)\}|$, solid curves) and from the approximated one ($I(\mathbf{r}, \mathbf{r}_E, \omega_E) \approx |\text{Re}\{G_{rr}(\mathbf{r}, \mathbf{r}_E, \omega_E)\} + i\text{Im}\{G_{rr}(\mathbf{r}, \mathbf{r}_E, \omega_E)\}|$, dashed curves). We have chosen two emission wavelengths and two different radii ($R = 80$ nm in panel (a) and $R = 45$ nm in panel (b)). For all curves we observe how the difference between the exact and approximated values increases for smaller distances and becomes negligible for large ones. Moreover the deviation is larger in the case of smaller GNSs,³⁵ as the comparison between panels (a) and (b) shows. In addition, the contribution of the off-resonant frequencies is more important for increasing wavelengths. For instance at $\lambda = 800$ nm (blue curves) and at an observation distance of 20 nm from the GNS surface, it amounts to 27% and 42% of G_{rr} for $R = 80$ nm and $R = 45$ nm, respectively. Hence, the full frequency integral has been used in the analysis of the electromagnetic near fields in the manuscript (see Fig. 4), otherwise the far-field approximation has been imposed for numerical efficiency (see Figs. 1-3).

Appendix B: Evaluation of the normally-ordered electric field variance

We now derive the expressions in Eqs. (1) and (2). Defining a general quadrature operator of the electric field as $\hat{\mathbf{E}}_\Theta = e^{i\Theta}\hat{\mathbf{E}}^{(+)} + e^{-i\Theta}\hat{\mathbf{E}}^{(-)}$, we write its variance $\langle \hat{\mathbf{E}}_\Theta^2 \rangle - \langle \hat{\mathbf{E}}_\Theta \rangle^2$ in normal order ($\langle : \cdot : \rangle$) as

$$\begin{aligned} \langle : [\Delta \hat{\mathbf{E}}_\Theta(\mathbf{r}, t)]^2 : \rangle &= e^{i2\Theta} \langle [\hat{\mathbf{E}}^{(+)}(\mathbf{r}, t)]^2 \rangle + e^{-i2\Theta} \langle [\hat{\mathbf{E}}^{(-)}(\mathbf{r}, t)]^2 \rangle - 2\text{Re}\{e^{i2\Theta} \langle \hat{\mathbf{E}}^{(+)}(\mathbf{r}, t) \rangle^2\} \\ &\quad + 2\langle \hat{\mathbf{E}}^{(-)}(\mathbf{r}, t) \hat{\mathbf{E}}^{(+)}(\mathbf{r}, t) \rangle - 2\langle \hat{\mathbf{E}}^{(-)}(\mathbf{r}, t) \rangle \langle \hat{\mathbf{E}}^{(+)}(\mathbf{r}, t) \rangle, \end{aligned} \quad (\text{B1})$$

where $\hat{\mathbf{E}}^{(-)} = (\hat{\mathbf{E}}^{(+)})^\dagger$ corresponds to the negative-frequency electric field. Next we use Eqs. (A5)-(A7) in Eq. (B1) to obtain the normally-ordered variance for the i th-component of the electric field quadrature

$$\langle : [\Delta \hat{E}_{i,\Theta}(\mathbf{r}, t)]^2 : \rangle = 2|g_i(\mathbf{r})|^2 \left[\langle (\hat{\sigma}^\dagger(t)\hat{\sigma}(t)) - |\hat{\sigma}(t)|^2 \rangle - \text{Re}\{e^{i2(\Theta+\phi_i)} \langle \hat{\sigma}(t) \rangle^2\} \right] = |g_i(\mathbf{r})|^2 \langle : [\Delta \hat{\sigma}_{\Theta+\phi_i}]^2 : \rangle, \quad (\text{B2})$$

which for $\Theta = 0$ gives Eq. (1), where we have simplified the notation by introducing the symbol $(\Delta \hat{\mathcal{E}}_i(\mathbf{r}, t))^2$. Here $\langle : [\Delta \hat{\sigma}_{\Theta+\phi_i}]^2 : \rangle$ denotes the general normally-ordered variance of the TLS coherence quadrature operator, $\hat{\sigma}_\Theta = e^{i\Theta}\hat{\sigma} + e^{-i\Theta}\hat{\sigma}^\dagger$, evaluated at the angle $\Theta + \phi_i$.

The variance in Eq. (B2) can be evaluated starting from the expectation value of the slowly varying coherence $\langle \hat{\sigma}(t) \rangle = \langle \hat{\sigma}(t) \rangle e^{i\omega_L t}$ in the co-rotating frame, which is governed by modified optical Bloch equations^{30,37}

$$\partial_t \langle \hat{\sigma}(t) \rangle = \left(-\frac{\gamma}{2} - \gamma^* + i\delta_L \right) \langle \hat{\sigma}(t) \rangle - i\frac{\Omega}{2} \langle \hat{\sigma}_z(t) \rangle, \quad (\text{B3})$$

$$\partial_t \langle \hat{\sigma}_z(t) \rangle = i \left(\Omega \langle \hat{\sigma}^\dagger(t) \rangle - \Omega^* \langle \hat{\sigma}(t) \rangle \right) - \gamma(1 + \langle \hat{\sigma}_z(t) \rangle), \quad (\text{B4})$$

where $\Omega = 2\mathbf{d} \cdot \langle \hat{\mathbf{E}}_{\text{free}}^{(+)}(\mathbf{r}_E) \rangle / \hbar = |\Omega|e^{i\phi_L}$ is the Rabi frequency and includes the local driving field enhancement due to the GNS.³⁸ The spontaneous decay rate is $\gamma = \frac{2\omega_E^2}{\hbar\epsilon_0 c^2} \mathbf{d} \cdot \text{Im}\{\mathbf{G}(\mathbf{r}_E, \mathbf{r}_E, \omega_E)\} \cdot \mathbf{d}$, γ^* is the pure dephasing rate, and $\delta_L = \omega_L - \tilde{\omega}_E$ is the detuning with respect to the dressed transition frequency $\tilde{\omega}_E = \omega_E - \frac{\mathcal{P}}{\pi\hbar\epsilon_0} \int_0^\infty d\omega [\frac{\omega^2}{c^2} \mathbf{d} \cdot \text{Im}\{\mathbf{G}(\mathbf{r}_E, \mathbf{r}_E, \omega)\} \cdot \mathbf{d} / (\omega - \omega_E)]$. From the steady-state condition of Eqs. (B3) and (B4), we deduce the stationary expectation value of the slow varying coherence $\langle \hat{\sigma} \rangle_s$ and population $\langle \hat{\sigma}_z \rangle_s$

$$\langle \hat{\sigma} \rangle_s = \frac{-\Omega[2\delta_L - i(\gamma + 2\gamma^*)]}{4\delta_L^2 + 2|\Omega|^2(1 + \frac{2\gamma^*}{\gamma}) + (\gamma + 2\gamma^*)^2} = e^{i[\phi_L + \phi_{\text{dep}}]} \sqrt{\frac{1}{2(1+x)}} \frac{z(\sqrt{\delta^2 + 1})}{1 + \delta^2 + z^2}, \quad (\text{B5})$$

$$\langle \hat{\sigma}_z \rangle_s = -1 + i \left(\frac{\Omega}{\gamma} \langle \hat{\sigma}^\dagger(\infty) \rangle - \frac{\Omega^*}{\gamma} \langle \hat{\sigma}(\infty) \rangle \right) = -\frac{1 + \delta^2}{1 + \delta^2 + z^2}, \quad (\text{B6})$$

in which we have used the normalized Rabi frequency $z = \sqrt{2}|\Omega|/\sqrt{\gamma(\gamma + 2\gamma^*)}$, the coherence dephasing phase $\phi_{\text{dep}} = \arctan[-(\gamma + 2\gamma^*)/(2\delta_L)]$, the normalized pure dephasing $x = 2\gamma^*/\gamma$, and the normalized detuning $\delta = 2\delta_L/(\gamma + 2\gamma^*)$. Notice that the normalized detuning and normalized Rabi frequency can be written in terms of the free-space normalized variables δ_0 and z_0 as $\delta = [\delta_0 - 2(\omega_E - \tilde{\omega}_E)/\gamma_0]/[(\gamma/\gamma_0)(1+x)]$ and $z = z_0|\Omega|/[|\Omega_0|(\gamma/\gamma_0)\sqrt{(1+x)}]$, respectively, where γ_0 is the decay rate and Ω_0 the Rabi frequency in free space. Using the results of Eqs. (B5) and (B6) and the stationary expectation value of the coherence $\langle \hat{\sigma} \rangle_s = \langle \hat{\sigma} \rangle_s e^{-i\omega_L t}$, we obtain the general normally-ordered atomic variance

$$\begin{aligned} \langle : [\Delta \hat{\sigma}_\Theta]^2 : \rangle &= 2 \left(\langle \hat{\sigma}^\dagger \hat{\sigma} \rangle_s - |\langle \hat{\sigma} \rangle_s|^2 \right) - 2\text{Re}\{e^{i2\Theta} \langle \hat{\sigma} \rangle_s^2\} \\ &= (1 + \langle \hat{\sigma}_z \rangle_s) - 2|\langle \hat{\sigma} \rangle_s|^2 - 2\text{Re}\{e^{i2\Theta} \langle \hat{\sigma} \rangle_s^2\} \\ &= \frac{z^2}{1 + \delta^2 + z^2} \left\{ 1 - \frac{1}{1+x} \frac{(\delta^2 + 1)[1 + \cos(2\Theta + 2\phi_L + 2\phi_{\text{dep}} - 2\omega_L t)]}{1 + \delta^2 + z^2} \right\}, \end{aligned} \quad (\text{B7})$$

in which we have used the general property $[\langle \hat{\sigma}^\dagger \hat{\sigma} \rangle = (1 + \langle \hat{\sigma}_z \rangle)/2]$ for a TLS, that is derived from the commutators $[\hat{\sigma}^\dagger, \hat{\sigma}] = \hat{\sigma}_z$ and the anti-commutation relation $\{\hat{\sigma}^\dagger, \hat{\sigma}\} = \mathbb{I}$. In general, Θ represents the phase of the electric field quadrature plus any propagative phase of g_i , ϕ_L is the phase of the driving field at \mathbf{r}_E , which is affected by the GNS, and ϕ_{dep} is the phase of the steady-state coherence $\langle \hat{\sigma} \rangle_s$. Equation (B2) for $\Theta = 0$ together with Eq. (B7) for $\Theta = \phi_i$ give the desired Eq. (2), where we denote $\langle : [\Delta \hat{E}_{i,0}(\mathbf{r}, t)]^2 : \rangle \equiv (\Delta \hat{\mathcal{E}}_i(\mathbf{r}, t))^2$ for brevity. Squeezing occurs if Eq. (B7) takes negative values. For the optimal condition when the cosine is equal to 1, this leads to the following threshold for the driving intensity

$$z^2 < (1 + \delta^2) \frac{1-x}{1+x}, \quad (\text{B8})$$

which is discussed in the main text.

Appendix C: Electric field variance from detection measurements

The measurement of squeezed light is associated with the photon correlations that are obtained from the counting statistics of photodetectors. Balanced homodyne detection is a well-established experimental procedure for measuring the correlation $\langle : [\Delta \hat{\mathbf{E}}_{\Theta}(\mathbf{r}, t)]^2 : \rangle$.^{11,39-41} Typically, in the homodyne detection scheme, the source field in Eq. (A2) is mixed by a beam splitter with a local oscillator, namely a high-intensity coherent field. This is a laser field $\hat{\mathbf{E}}_{\text{free}}^{(+)}(\mathbf{r}, t) |\alpha\rangle = |\alpha| e^{i(\phi_L - \omega_L t)} |\alpha\rangle$, where $|\alpha\rangle$ is a coherent state of amplitude $|\alpha|$ and well-defined phase ϕ_L at the photodetector, so that fluctuations are due to shot noise, *i.e.*, $\langle : \Delta \hat{\mathbf{E}}_{\text{free}} : \rangle = 0$. Note that in the setup sketched in Fig. 1a, the total field is actually a superposition of $\hat{\mathbf{E}}_{\text{free}}(\mathbf{r}, t)$ and the source field $\hat{\mathbf{E}}(\mathbf{r}, t)$, so that it already contains the local oscillator and does not require a beam splitter. Assuming that the coherent field is much stronger than the source field $\hat{\mathbf{E}}_{\text{free}}(\mathbf{r}, t) \gg \hat{\mathbf{E}}(\mathbf{r}, t)$, one can derive the variance of the photocounts $\overline{\Delta n}$ for a detector within the short time interval Δt

$$\overline{\Delta n}^2 = \xi \Delta t |\alpha|^2 + \xi^2 \Delta t^2 |\alpha|^2 \langle : [\Delta \hat{\mathbf{E}}_{-\phi_L + \omega_L t}(\mathbf{r}, t)]^2 : \rangle, \quad (\text{C1})$$

where ξ is the detector efficiency. From Eq. (C1), it is inferred that $\langle : \Delta [\hat{\mathbf{E}}_{-\phi_L + \omega_L t}(\mathbf{r}, t)]^2 : \rangle$ is obtained by subtracting and normalizing the detected shot noise $\bar{n} = \xi \Delta t |\alpha|^2$, which provides (see the derivation in Appendix C1)

$$\frac{\overline{\Delta n}^2 - \bar{n}}{\bar{n}} = \xi \Delta t \langle : [\Delta \hat{\mathbf{E}}_{-\phi_L + \omega_L t}(\mathbf{r}, t)]^2 : \rangle. \quad (\text{C2})$$

The scattered field is squeezed if this magnitude has a negative value, *i.e.*, it features reduced quantum fluctuations with respect to shot noise, which is proportional to $|g_i(\mathbf{r})|^2$ as inferred from Eq. (B2). Moreover, the phase of the laser can be varied in the far field in order to fix the phase in Eq. (B7) and maximize the cosine, *i.e.*, maximize the degree of squeezing.

1. Derivation of Equation (C2)

In order to derive Eq. (C2) we need the mean number of photocounts in the time interval Δt . Using a detector with efficiency ξ this quantity reads¹⁶

$$\begin{aligned} \bar{n} &= \xi \Delta t \langle \hat{\mathbf{E}}_{\text{tot}}^{(-)}(\mathbf{r}, t) \hat{\mathbf{E}}_{\text{tot}}^{(+)}(\mathbf{r}, t) \rangle, \\ &= \xi \Delta t \left(\langle \hat{\mathbf{E}}_{\text{free}}^{(-)}(\mathbf{r}, t) \hat{\mathbf{E}}_{\text{free}}^{(+)}(\mathbf{r}, t) \rangle + \langle \hat{\mathbf{E}}^{(-)}(\mathbf{r}, t) \hat{\mathbf{E}}^{(+)}(\mathbf{r}, t) \rangle + \langle \hat{\mathbf{E}}_{\text{free}}^{(-)}(\mathbf{r}, t) \hat{\mathbf{E}}^{(+)}(\mathbf{r}, t) \rangle + \langle \hat{\mathbf{E}}^{(-)}(\mathbf{r}, t) \hat{\mathbf{E}}_{\text{free}}^{(+)}(\mathbf{r}, t) \rangle \right). \end{aligned} \quad (\text{C3})$$

Here, we used the free and source field notation of Eq. (A2). If we introduce the density matrix $\hat{\rho} = \hat{\sigma} |\alpha\rangle \langle \alpha|$ to describe a disentangled emitter-field system at equal times, Eq. (C3) becomes

$$\bar{n} = \xi \Delta t \left(|\alpha|^2 + \langle \hat{\mathbf{E}}^{(-)} \hat{\mathbf{E}}^{(+)} \rangle + |\alpha| e^{-i(\phi_L + \omega_L t)} \langle \hat{\mathbf{E}}^{(+)} \rangle + |\alpha| e^{i(\phi_L - \omega_L t)} \langle \hat{\mathbf{E}}^{(-)} \rangle \right). \quad (\text{C4})$$

If we further assume that $|\alpha|^2 \gg \langle \hat{\mathbf{E}}^{(-)} \hat{\mathbf{E}}^{(+)} \rangle$, the number of photocounts is mainly determined by the laser field

$$\bar{n} = \xi \Delta t |\alpha|^2. \quad (\text{C5})$$

Moreover, we need the variance in the number of photocounts, which follows from statistical considerations¹⁶

$$\overline{\Delta n}^2 = \bar{n} + \xi^2 (\Delta t)^2 \langle : [\Delta \hat{\mathbf{I}}(\mathbf{r}, t)]^2 : \rangle, \quad (\text{C6})$$

where $\hat{\mathbf{I}}(\mathbf{r}, t) = \hat{\mathbf{E}}_{\text{tot}}^{(-)}(\mathbf{r}, t) \hat{\mathbf{E}}_{\text{tot}}^{(+)}(\mathbf{r}, t)$ is the first-order intensity correlation. To evaluate Eq. (C6) we write the intensity variance explicitly

$$\Delta \hat{\mathbf{I}}(\mathbf{r}, t) = \Delta \{ \hat{\mathbf{E}}^{(-)}(\mathbf{r}, t) \hat{\mathbf{E}}^{(+)}(\mathbf{r}, t) \} + \Delta \{ \hat{\mathbf{E}}_{\text{free}}^{(-)}(\mathbf{r}, t) \hat{\mathbf{E}}_{\text{free}}^{(+)}(\mathbf{r}, t) \} + \Delta \{ \hat{\mathbf{E}}^{(-)}(\mathbf{r}, t) \hat{\mathbf{E}}_{\text{free}}^{(+)}(\mathbf{r}, t) + \hat{\mathbf{E}}_{\text{free}}^{(-)}(\mathbf{r}, t) \hat{\mathbf{E}}^{(+)}(\mathbf{r}, t) \}, \quad (\text{C7})$$

and

$$\begin{aligned} [\Delta \hat{\mathbf{I}}(\mathbf{r}, t)]^2 &= [\Delta \{ \hat{\mathbf{E}}^{(-)} \hat{\mathbf{E}}^{(+)} \}]^2 + [\Delta \{ \hat{\mathbf{E}}_{\text{free}}^{(-)} \hat{\mathbf{E}}_{\text{free}}^{(+)} \}]^2 + [\Delta \{ \hat{\mathbf{E}}^{(-)} \hat{\mathbf{E}}_{\text{free}}^{(+)} + \hat{\mathbf{E}}_{\text{free}}^{(-)} \hat{\mathbf{E}}^{(+)} \}]^2 + \\ &\quad \Delta \{ \hat{\mathbf{E}}^{(-)} \hat{\mathbf{E}}^{(+)} \} \Delta \{ \hat{\mathbf{E}}_{\text{free}}^{(-)} \hat{\mathbf{E}}_{\text{free}}^{(+)} \} + \Delta \{ \hat{\mathbf{E}}_{\text{free}}^{(-)} \hat{\mathbf{E}}_{\text{free}}^{(+)} \} \Delta \{ \hat{\mathbf{E}}^{(-)} \hat{\mathbf{E}}^{(+)} \} + \\ &\quad \Delta \{ \hat{\mathbf{E}}^{(-)} \hat{\mathbf{E}}^{(+)} \} \Delta \{ \hat{\mathbf{E}}^{(-)} \hat{\mathbf{E}}_{\text{free}}^{(+)} + \hat{\mathbf{E}}_{\text{free}}^{(-)} \hat{\mathbf{E}}^{(+)} \} + \Delta \{ \hat{\mathbf{E}}^{(-)} \hat{\mathbf{E}}_{\text{free}}^{(+)} + \hat{\mathbf{E}}_{\text{free}}^{(-)} \hat{\mathbf{E}}^{(+)} \} \Delta \{ \hat{\mathbf{E}}^{(-)} \hat{\mathbf{E}}^{(+)} \} + \\ &\quad \Delta \{ \hat{\mathbf{E}}_{\text{free}}^{(-)} \hat{\mathbf{E}}_{\text{free}}^{(+)} \} \Delta \{ \hat{\mathbf{E}}^{(-)} \hat{\mathbf{E}}_{\text{free}}^{(+)} + \hat{\mathbf{E}}_{\text{free}}^{(-)} \hat{\mathbf{E}}^{(+)} \} + \Delta \{ \hat{\mathbf{E}}^{(-)} \hat{\mathbf{E}}_{\text{free}}^{(+)} + \hat{\mathbf{E}}_{\text{free}}^{(-)} \hat{\mathbf{E}}^{(+)} \} \Delta \{ \hat{\mathbf{E}}_{\text{free}}^{(-)} \hat{\mathbf{E}}_{\text{free}}^{(+)} \}. \end{aligned} \quad (\text{C8})$$

Introducing this last expression in Eq. (C6) and using the density matrix $\hat{\rho} = \hat{\sigma} |\alpha\rangle\langle\alpha|$, we find the expectation value

$$\begin{aligned} \overline{n}^2 = & \bar{n} + \xi^2 \Delta t^2 \left(\langle :[\Delta\{\hat{\mathbf{E}}^{(-)}\hat{\mathbf{E}}^{(+)}\}]^2 : \rangle + |\alpha|^2 \langle :[\Delta\{\hat{\mathbf{E}}^{(-)}e^{i(\phi_L - \omega_L t)} + e^{-i(\phi_L + \omega_L t)}\hat{\mathbf{E}}^{(+)}\}]^2 : \rangle + \right. \\ & \left. 2|\alpha| \langle :[\Delta\{\hat{\mathbf{E}}^{(-)}\hat{\mathbf{E}}^{(+)}\} \Delta\{\hat{\mathbf{E}}^{(-)}e^{i(\phi_L - \omega_L t)} + e^{-i(\phi_L + \omega_L t)}\hat{\mathbf{E}}^{(+)}\}] : \rangle \right), \end{aligned} \quad (\text{C9})$$

where we have used the fact that the correlations $\langle :[\Delta\{\hat{\mathbf{E}}_{\text{free}}^{(-)}\hat{\mathbf{E}}_{\text{free}}^{(+)}\}] : \rangle = 0$ due to the coherent character of the free field. If we assume the same conditions considered for deriving Eq. (C5), then the third term in Eq. (C9) dominates and we obtain

$$\overline{n}^2 = \bar{n} + \xi^2 (\Delta t)^2 |\alpha|^2 \langle :[\Delta\{\hat{\mathbf{E}}^{(-)}e^{i(\phi_L - \omega_L t)} + e^{-i(\phi_L + \omega_L t)}\hat{\mathbf{E}}^{(+)}\}]^2 : \rangle, \quad (\text{C10})$$

from which we deduce the correlation formula of Eq. (C2).

-
- ¹ L. Novotny and N. van Hulst, *Nat. Photon.* **5**, 83 (2011).
 - ² K. Kneipp, Y. Wang, H. Kneipp, L. T. Perelman, I. Itzkan, R. R. Dasari, and M. S. Feld, *Phys. Rev. Lett.* **78**, 1667 (1997).
 - ³ P. Anger, P. Bharadwaj, and L. Novotny, *Phys. Rev. Lett.* **96**, 113002 (2006).
 - ⁴ S. Kühn, U. Håkanson, L. Rogobete, and V. Sandoghdar, *Phys. Rev. Lett.* **97**, 017402 (2006).
 - ⁵ M. Tame, K. McEnery, Ş. Özdemir, J. Lee, S. Maier, and M. Kim, *Nature Phys.* **9**, 329 (2013).
 - ⁶ J.-M. Raimond and S. Haroche, *Exploring the quantum* (Oxford University Press, Oxford, UK, 2006).
 - ⁷ A. V. Akimov, A. Mukherjee, C. L. Yu, D. E. Chang, A. S. Zibrov, P. R. Hemmer, H. Park, and M. D. Lukin, *Nature* **450**, 402 (2007).
 - ⁸ S. Schietinger, M. Barth, T. Aichele, and O. Benson, *Nano Lett.* **9**, 1694 (2009).
 - ⁹ A. Huck, S. Kumar, A. Shakoob, and U. L. Andersen, *Phys. Rev. Lett.* **106**, 096801 (2011).
 - ¹⁰ D. F. Walls and P. Zoller, *Phys. Rev. Lett.* **47**, 709 (1981).
 - ¹¹ A. Ourjoumtsev, A. Kubanek, M. Koch, C. Sames, P. W. H. Pinkse, G. Rempe, and K. Murr, *Nature* **474**, 623 (2011).
 - ¹² D. F. Walls, *Nature* **306**, 141 (1983).
 - ¹³ A. H. Safavi-Naeini, S. Groblacher, J. T. Hill, J. Chan, M. Aspelmeyer, and O. Painter, *Nature* **500**, 185 (2013).
 - ¹⁴ R. Loudon and P. L. Knight, *J. Mod. Opt.* **34**, 709 (1987).
 - ¹⁵ C. Stehle, H. Bender, C. Zimmermann, D. Kern, M. Fleischer, and S. Slama, *Nat. Photon.* **5**, 494 (2011).
 - ¹⁶ W. Vogel and D.-G. Welsch, *Quantum optics* (WILEY-VCH Verlag, Weinheim, DE, 2006).
 - ¹⁷ C. Tai, *Dyadic Green Functions in Electromagnetic Theory* (IEEE Press, New Jersey, 1996).
 - ¹⁸ The cosine in Eq. (2) contains phases originating from scattering off the nanostructure and from the evolution of the coherence operator, and can always be set to unity, for instance by choosing an appropriate homodyne scheme for the detection of squeezing (see Appendix C). Therefore, without loss of generality, we impose this in the numerical evaluations.
 - ¹⁹ H. T. Dung, L. Knöll, and D.-G. Welsch, *Phys. Rev. A* **65**, 043813 (2002).
 - ²⁰ C. F. Bohren and D. R. Huffman, *Absorption and Scattering of Light by Small Particles* (John Wiley & Sons, New York, 1983).
 - ²¹ A. G. Curto, G. Volpe, T. H. Taminiau, M. P. Kreuzer, R. Quidant, and N. F. van Hulst, *Science* **329**, 930 (2010).
 - ²² A. Batalov, C. Zierl, T. Gaebel, P. Neumann, I.-Y. Chan, G. Balasubramanian, P. R. Hemmer, F. Jelezko, and J. Wrachtrup, *Phys. Rev. Lett.* **100**, 077401 (2008).
 - ²³ The condition for squeezing, *i.e.* $(\Delta\hat{\mathcal{E}}_i(\mathbf{r}, t))^2 < 0$ in Eq. (2), sets an upper limit for the driving field intensity, $z^2 < (1 + \delta^2)(1 - x)/(1 + x)$. Notice that this requirement cannot be fulfilled for $x \geq 1$, which already occurs for pure dephasing larger than half the spontaneous decay rate.
 - ²⁴ L. Rogobete, F. Kaminski, M. Agio, and V. Sandoghdar, *Opt. Lett.* **32**, 1623 (2007).
 - ²⁵ J. D. Jackson, *Classical Electrodynamics*, 3rd ed. (John Wiley & Sons, New York, 1999).
 - ²⁶ A. Huck, S. Smolka, P. Lodahl, A. S. Sørensen, A. Boltasseva, J. Janousek, and U. L. Andersen, *Phys. Rev. Lett.* **102**, 246802 (2009).
 - ²⁷ M. A. Taylor, J. Janousek, V. Daria, J. Knittel, B. Hage, H. A. Bachor, and W. P. Bowen, *Nat. Photon.* **7**, 229 (2013).
 - ²⁸ A. Gonzalez-Tudela, D. Martín-Cano, E. Moreno, L. Martín-Moreno, C. Tejedor, and F. J. Garcia-Vidal, *Phys. Rev. Lett.* **106**, 020501 (2011).
 - ²⁹ M. Gullans, T. G. Tiecke, D. E. Chang, J. Feist, J. D. Thompson, J. I. Cirac, P. Zoller, and M. D. Lukin, *Phys. Rev. Lett.* **109**, 235309 (2012).
 - ³⁰ L. Knöll, S. Scheel, and D.-G. Welsch, "Coherence and statistics of photons and atoms," (Wiley, New York, 2001) Chap. QED in dispersing and absorbing dielectric media, pp. 1–60.
 - ³¹ H. T. Dung, L. Knöll, and D.-G. Welsch, *Phys. Rev. A* **64**, 013804 (2001).
 - ³² L.-W. Li, P.-S. Kooi, M.-S. Leong, and T.-S. Yee, *IEEE Trans. Microw. Theory Techn.* **42**, 2302 (1994).
 - ³³ D. R. Lide, ed., *CRC Handbook of Chemistry and Physics*, 87th ed. (CRC Press, Boca Raton, FL, 2006).
 - ³⁴ F. Kaminski, V. Sandoghdar, and M. Agio, *J. Comput. Theor. Nanosci.* **4**, 635 (2007).
 - ³⁵ H. T. Dung, L. Knöll, and D.-G. Welsch, *Phys. Rev. A* **66**, 063810 (2002).

- ³⁶ D. Dzsoſtjan, J. Käſtel, and M. Fleiſchhauer, Phys. Rev. B **84**, 075419 (2011).
- ³⁷ X.-W. Chen, V. Sandoghdar, and M. Agio, Phys. Rev. Lett. **110**, 153605 (2013).
- ³⁸ N. M. Mojarad, V. Sandoghdar, and M. Agio, J. Opt. Soc. Am. B **25**, 651 (2008).
- ³⁹ L. Mandel, Phys. Rev. Lett. **49**, 136 (1982).
- ⁴⁰ W. Vogel, Phys. Rev. Lett. **67**, 2450 (1991).
- ⁴¹ M. Collett, D. Walls, and P. Zoller, Opt. Commun. **52**, 145 (1984).